ACS OMEGA

Open Access

http://pubs.acs.org/journal/acsodf

Article

Antibiofilm Activity of PDMS/TiO_2 against *Candida glabrata* through Inhibited Hydrophobic Recovery

Khoi-Nguyen Nguyen, Leena Sao, Kevin Kyllo, Danitza Hernandez, Samantha Salomon, Kalp Shah, Dahyun Oh,* and Katy C. Kao*

Cite This: *ACS Omega* 2024, 9, 42593−42601

Read Online

ACCESS | Metrics & More | Article Recommendations | Supporting Information

ABSTRACT: Coatings with antibiofilm properties are desirable for biomedical applications. Titanium dioxide (TiO_2) has been explored as an antimicrobial agent in materials development primarily due to it being an excellent photocatalyst. *Candida glabrata* (*C. glabrata*) is an emerging human fungal pathogen with known high resistance to oxidative stress. Here, we fabricated a polydimethylsiloxane/titanium dioxide (PDMS/TiO_2) nanocomposite coating and tested its antibiofilm activities against *C. glabrata*. The resulting nanocomposite exhibited >50% reduction in *C. glabrata* biofilm formation with 2.5 wt % TiO_2 loading, even in the dark. Through ROS detection and surface characterization, the antibiofilm activity was attributed to the synergistic interaction of TiO_2 nanoparticles with the PDMS matrix, which resulted in the impediment of hydrophobic recovery. This work provides a design strategy to develop antibiofilm coatings against *C. glabrata*.

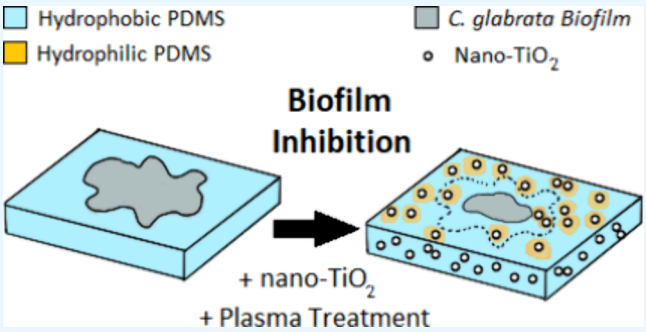

INTRODUCTION

Biofilm formation serves as a crucial virulence mechanism to resist both host immune responses and antifungal treatments on both biological and abiotic surfaces.[1−3] Surface engineering can effectively prevent the biofilm formation by inhibiting fungal cell adhesion to surfaces. Initial cell adhesion is pivotal for the proliferation of pathogens including the emerging fungal pathogen such as *Candida glabrata* (*C. glabrata*) in biofilms. The development of antifungal drugs is hindered due to the challenge in targeting fungal cells specifically without affecting human cells.[4] The presence of biofilms exacerbates this issue by imparting significant drug resistance, which leads to high failure rates of antifungal treatments of up to 70%.[5−9] This limitation underscores the urgent need for developing antibiofilm coatings as an alternative approach to mitigate biofilm-associated infections. Thus, the application of antibiofilm coatings or the modification of existing abiotic surfaces holds significant promise in impeding the proliferation of *C. glabrata*.

Surface properties including surface roughness and wettability have been found to influence microbial cell surface attachment.[10] Le et al. studied the effects of the surface architecture on *C. albicans* biofilm formation using polished or unpolished titanium and glass surfaces; they found biofilm formation to be higher on surfaces with higher roughness and not correlated with wettability.[11] Another study using acrylic resin surfaces found surface roughness to have no effect on *C. albicans* and *C. glabrata* biofilm formation, but coating with either zwitterionic or hydrophilic compounds led to reduced cell adhesion.[12]

Nanomaterials, such as TiO_2, have been explored as antimicrobial materials that can potentially prevent and reduce formation of bacterial and fungal biofilms on surfaces.[9,13−17] The mechanism behind the antimicrobial activity of TiO_2 has been attributed to the photoactivated formation of reactive oxygen species (ROS). The presence of ROS induces oxidative stress and damages cell membranes on a wide range of pathogenic microorganisms.[18] Studies have also shown gene expression changes in bacteria induced by UV-activated TiO_2-based nanomaterials, suggesting disruptions in metabolism and activation of cellular detoxification and repair.[19,20] Interestingly, some studies have shown antimicrobial activity of TiO_2 without UV exposure as well. Wasa et al.[21] found that a nanostructured anatase−rutile-carbon TiO_2 coating inhibited the growth of *Escherichia coli*, *Staphylococcus aureus*, *Pseudomonas aeruginosa*, and *Saccharomyces cerevisiae* without UV light exposure (in visible light or dark), demonstrating that TiO_2 nanomaterials exert additional antimicrobial mechanisms besides photoactivated ROS generation. These mixed results

Received: August 26, 2024
Revised: September 17, 2024
Accepted: September 25, 2024
Published: October 3, 2024

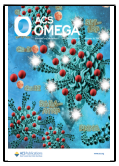

indicate the need for a systematic investigation into the surface properties that influence *C. glabrata* biofilm formation, aiding in the design of materials capable of preventing biofilm development.

In this work, we explore the antibiofilm effect of the TiO_2/polydimethylsiloxane (PDMS) nanocomposite against *C. glabrata*. PDMS is a commonly used material in biomedical applications due to safety, stability, and cost considerations. Studies have focused on the modifications of PDMS to enhance its antimicrobial properties.[22−24] We incorporated anatase TiO_2 nanoparticles (NP) into PDMS matrices with different concentrations of TiO_2 and analyzed their surface properties to unravel their antibiofilm activity mechanism. Composite films consisting of TiO_2 NP embedded in PDMS were tested for ROS generation using methylene blue and evaluated for their ability to inhibit biofilm formation under both visible light or dark conditions. A possible ROS-independent mechanism for antibiofilm activity of the TiO_2/PDMS composite is proposed.

MATERIALS AND METHODS

Preparation of the 96-Well Plates with TiO_2 and PDMS Coating. The PDMS binder (Sylgard 184 silicone elastomer kit, Dow Corning) was prepared by mixing the PDMS elastomer base and curing agent with the weight ratio of 10:1 using a spatula for about 1 minute. Various concentrations of PDMS/TiO_2 solutions (2.5, 5, 9, and 13 wt % of TiO_2, 99% anatase, US Research Nanomaterials Inc., average particles size: 18 nm) were made by diluting the PDMS/TiO_2 mixture to 5 wt % in *tert*-butyl alcohol (TBA). The solution was vortexed for 1 minute and sonicated for 15 minute at 40 °C using a bath sonicator. After the sonication, the solution was vortexed again for 1 minute before loading on the well plate using a pipette. Each well of the 96-well plates was coated with 100 μL of the PDMS/TiO_2 solution and was cured at 80 °C for 30 minute in a vacuum oven. The 96-well plates were then treated with oxygen plasma (Nordson March CS-1701, 100 W, oxygen flow rate: 30 sccm) for 30 seconds.

Photocatalysis Experiment. PDMS-coated plates with different TiO_2 weight loadings were exposed to the light or kept in the dark. The LED lamp was placed 18 in. away from the plates. The LED lamp had a power rating of 8.3W, operating at 120 VAC, 60 Hz, and 0.07 A. To minimize evaporation during the experiment, water was added to the surrounding empty wells in the 96-well plates. In each coated well of the 96-well plates, 300 μL of 5 ppm methylene blue (MB, Sigma-Aldrich) solution was added. To obtain a baseline absorbance of the MB solution, the plates were then incubated at 37 °C for 10 minutes, after which the MB solution was removed, and the MB absorbance (665 nm) was measured using a plate reader (Tecan Infinite 200 PRO). The MB solution was then returned to the wells for a 24 hour incubation period at 37 °C, either under light exposure or in the dark. Following the incubation, the absorbance of the MB solution was measured again (representative absorbance spectra are included in Figure S1). To determine the percent reduction of the MB dye, individual well data were subjected to baseline correction. The corrected absorbance values were then used to calculate the percent MB dye reduction according to the following equation:

$$\text{Percentdyereduction} = \frac{A_{initial} - A_{final}}{A_{initial}} \times 100\% \quad (1)$$

where $A_{initial}$ is the initial absorbance value after the 10 minute incubation and A_{final} is the absorbance value obtained after the 24 hour incubation. The data were then statistically analyzed and compared between the different TiO_2 weight loadings and incubation conditions.

TiO_2 and PDMS Composite Characterization. *Scanning Electron Microscopy.* Scanning electron microscopy (SEM) was performed using an FEI Quanta 200 system. The PDMS/TiO_2 coatings were deposited onto silicon wafers and subsequently sputter-coated with gold.

Hydrophobicity Measurements. The static contact angles were measured using the drop shape analyzer (KRUSS DSA30M). Five drops of 4 μL deionized (DI) water were placed at different points on each coating sample. The contact angles were analyzed using KRUSS ADVANCE software. This process was repeated three times for each coating formulation.

Roughness Analysis. The surface roughness was determined with confocal laser scanning microscopy via a 3D surface profiler (Keyence VK-X3000) in the laser scanning mode (semiconductor laser 661 nm). The coating samples were cast onto polypropylene disks of 2 cm in diameter. Three measurements were performed at different locations on each sample, and the average area roughness values were obtained. The roughness parameters S_a and S_z were calculated using the associated software (VK-A3E) in accordance with ISO 25178. S_a is the arithmetical mean value of the absolute surface heights of the sample and S_z is the maximum height of the surface, which is the sum of the maximum peak heights and maximum valley depths of the sample.[25]

Strains and Growth Conditions. *C. glabrata* strains sMH080 (wild-type) and sMH081 (H_2O_2-resistant mutant) used in the study are derived from ATCC 2001.[26] Prior to the experiments, *C. glabrata* strains were cultured overnight in 10 mL of YPD (yeast peptone dextrose) media at 37 °C and 230 rpm.

Biofilm Quantification in TiO_2 NP-Coated 96-Well Plates. Overnight cultures were centrifuged at 2700 rpm for 5 minutes at room temperature and washed two times with 1× PBS (phosphate buffer saline). The cell pellet was resuspended in 10 mL of 1× PBS. The cell concentration was measured using the Invitrogen Countess II Automated Cell Counter (Thermo Fisher) and normalized to a concentration of 1×10^7 total cells/mL with RPMI 1640 media supplemented with 2% glucose and 34.53 g/L of MOPS (3-(N-morpholino) propanesulfonic acid) and buffered to pH 7.0 using 10 N NaOH.

One hundred microliters of the cell suspension was pipetted into each of the inner wells of the coated 96-well plate. To prevent edge effects due to evaporation, 100 μL of 1× PBS was pipetted into wells along the perimeter of the plate. The plates were incubated at 37 °C for 24 hours in light (under the LED lamp) or in the dark. After incubation, cell cultures were rinsed with 200 μL of 1× PBS to remove any nonadherent cells. One hundred fifty microliters of absolute methanol was added to each well. After 15 minutes, the methanol was removed and allowed to dry completely for 10 minutes. One hundred microliters of 0.1% crystal violet (CV) solution was added to each well and incubated at room temperature for 20 minutes. The plate was washed with DI water three times and allowed to air dry for 1 hours. Then, 150 μL of 33% acetic acid was added to each well. One hundred microliters of each sample

https://doi.org/10.1021/acsomega.4c07869
ACS Omega 2024, 9, 42593−42601

and 100 μL of DI water were transferred into a black well plate for absorbance measurements in a plate reader (BioTek Synergy Neo2Multi-Mode Microplate Reader) at 590 nm.

To calculate the percent biofilm inhibition compared to the control (samples without TiO_2), the following equation was used:

$$\text{Percent inhibition} = \left(\frac{C - X}{C}\right) \times 100\% \quad (2)$$

where C is the average absorbance of the control samples and X is the average absorbance value of the experimental samples. Student's t test was used to determine statistical significance between treatments.

RESULTS AND DISCUSSION

ROS Generation by the TiO_2 Nanocomposite Film in Visible Light and Dark. The photocatalytic performance of PDMS/TiO_2 nanocomposite films was evaluated by measuring the percentage reduction of the methylene blue (MB) dye in coatings with various nanoparticle weight loadings. The experiment was conducted under LED light irradiation or dark conditions over a 24 hour incubation period to estimate the production of reactive oxygen radicals in these conditions. Results demonstrated a TiO_2 concentration-dependent increase in MB dye reduction under LED exposure (Figure 1),

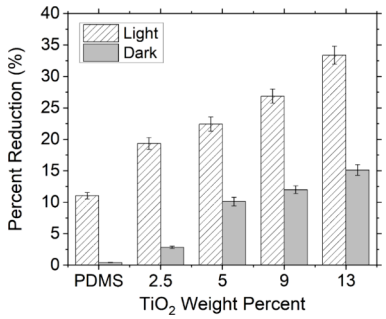

Figure 1. Percentage reduction of the MB dye in plasma-treated PDMS/TiO_2 coatings with various NP weight loadings under LED irradiation or dark conditions over a 24 hour incubation period. Error bars are standard errors between 4 replicates.

indicating photoactivation of the PDMS/TiO_2 nanocomposite coating in visible light.[27,28] Typically, anatase TiO_2 nanoparticles require incident light in the UV region for photoactivation due to their 3.2 eV bandgap.[29] However, introducing oxygen vacancies on the surface of the nanoparticles effectively enhances the photoactivity of anatase TiO_2.[30] TiO_2 nanomaterials enriched with oxygen vacancies can be obtained via synthesis,[31,32] ion sputtering,[30,33,34] annealing,[35] and oxygen plasma treatment.[36,37] These defects act as dissociative sites, transforming adsorbed O_2 and H_2O into radical superoxide ($\cdot O_2^-$) and hydroxyl groups ($\cdot$OH), respectively.[30,38−40] This mechanism explains the observed levels of MB reduction under dark conditions that correlated with the TiO_2 concentration (Figure 1), as the surface-bound radicals degrade MB through successive hydroxylation.[41]

Furthermore, the oxygen vacancies act as electron traps, effectively lowering the bandgap of anatase TiO_2.[42] Bi et al. demonstrated that introducing 7.8% oxygen vacancies in anatase TiO_2 nanoparticles through annealing could reduce the bandgap to 1.99 eV. These defect-rich TiO_2 nanoparticles exhibited remarkable efficiency in reducing NO and rhodamine B.[35] Similarly, the oxygen plasma treatment of the PDMS/TiO_2 nanocomposite coating in this work serves a dual function: it etches the topmost PDMS layer, thereby exposing the surface of TiO_2 particles, and creates oxygen vacancies in the TiO_2 nanoparticles.[36,37] This process increased the oxygen vacancy concentration in the TiO_2 nanoparticles, potentially lowering the bandgap and facilitating efficient photon absorption within the visible light spectrum.[35,36,43] Additionally, TiO_2 nanoparticles tend to self-aggregate, forming three-dimensional networks in the solution during the colloidal preparation of the prepolymer mixture. This self-aggregation behavior gives rise to the antenna effect, which enables efficient energy transfer along a chain of aggregated particles. As a result, the absorbed light energy can be transported to the active sites where it induces the desired chemical reactions, prolonging the useful lifetimes of photogenerated excitons and improving the photocatalytic performance of the TiO_2 nanoparticles in the network.[44]

Unexpectedly, a 10% ± 0.5% reduction in MB was also observed in the PDMS-only control samples under the LED condition. This phenomenon may be attributed to the destruction of methyl groups (Si−CH_3) along the siloxane backbone of PDMS, resulting in the subsequent formation of oxygen-containing groups such as silanol (Si−OH), alcohol (C−OH), and carboxylic acid (COOH) on the PDMS surface during the oxygen plasma treatment.[45,46] Under LED irradiation, these oxygen-containing groups, particularly silanol, interact with water molecules, generating reactive hydroxyl radicals.[47] Alberti et al. observed a similar phenomenon, where bare PDMS without TiO_2 addition exhibited some MB degradation under solar-simulated irradiation.[22]

Effects of PDMS/TiO_2 Nanocomposites on *C. glabrata* Biofilm Growth in Light and Dark Conditions. To explore whether the observed ROS formation in the PDMS/TiO_2 nanocomposite contributes to antimicrobial activities, the efficacy of the nanocomposite coating on inhibiting biofilm formation in *C. glabrata* was tested under LED and dark conditions. In the presence of TiO_2, significant reductions in biofilm growth compared to PDMS-only samples were observed regardless of light exposure. The levels of inhibition were similar between TiO_2 concentrations between 2.5 and 10%, with ∼51% inhibition and ∼56% inhibition observed in the presence and absence of light, respectively (see Figure 2A and Table 1). A slight decrease, although not statistically significant, in inhibition was observed when the TiO_2 concentration was increased to 13%. The observed biofilm inhibition activities of TiO_2 did not correlate with the TiO_2-dependent and light-dependent increase in ROS generation observed using MB, suggesting that ROS generation may not be the main contributor to the antibiofilm activity of the nanocomposite tested in this study.

To further investigate whether oxidative stress is involved in the antibiofilm activity of the TiO_2 nanocomposite, the strain (sMH081) with a mutation in *Ste11*, the mitogen-activated protein kinase (MAPK) previously shown to have a ∼10× increase in oxidative stress tolerance to hydrogen peroxide,[26] was tested for the ability to form biofilms on the TiO_2 nanocomposite. As shown in Figure 2, the TiO_2 nanocomposite had a similar antibiofilm activity against the oxidative stress-tolerant mutant sMH081 compared to the wild-type strain in both LED and dark conditions. This result further suggests that oxidative stress is likely not involved in

https://doi.org/10.1021/acsomega.4c07869
ACS Omega 2024, 9, 42593−42601

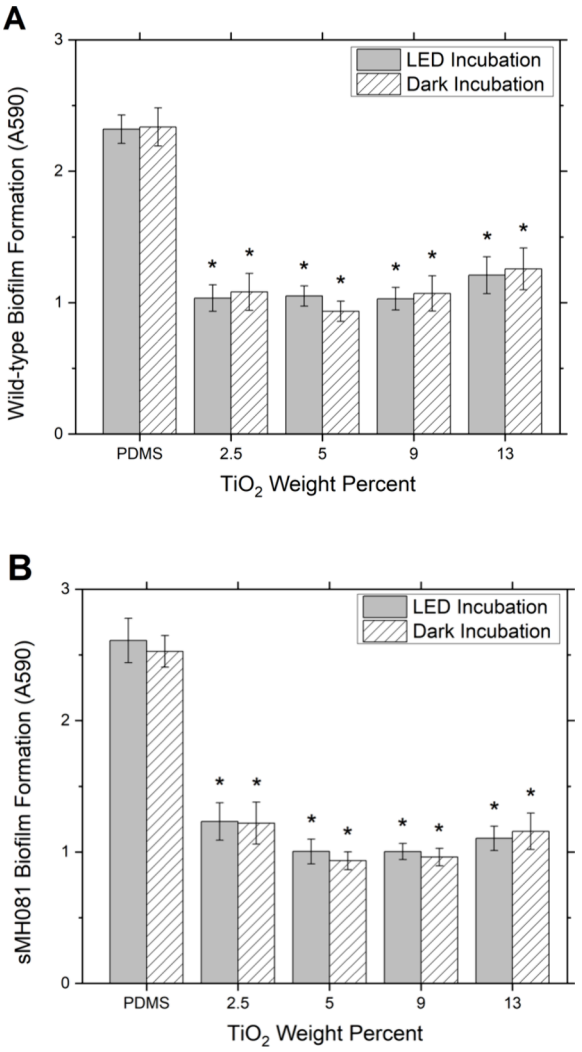

Figure 2. Biofilm formation (A: sMH080 [wild-type] and B: sMH081 [oxidative stress-tolerant mutant]) on plasma-treated plates with various TiO_2 NP concentrations under LED and dark incubation. Error bars are standard errors from four biological replicates. *: statistically different from its PDMS-only control (p-value < 0.05, Student's t test).

Table 1. Biofilm Inhibition (%) in Different Concentrations of TiO_2 (wt %) in the Wild-Type Strain

condition	PDMS-only	2.5%	5%	9%	13%
LED	0	52.6 ± 6	51.5 ± 5	52.3 ± 5	44.7 ± 7
dark	0	50.4 ± 7	56.2 ± 6	48.9 ± 8	41.2 ± 9

the antibiofilm activity of the TiO_2 nanocomposite. *C. glabrata* is known to have high resistance to oxidative stress,[48−51] which may explain the lack of susceptibility to ROS generated by the TiO_2 nanocomposite. Instead, the surface properties of the nanomaterial may be responsible for the observed antibiofilm properties.

Surface Characterization of the Nanocomposite. The SEM analysis of the nanocomposite coatings with different TiO_2 weight loadings revealed interesting trends in the surface morphology of the coatings (Figures 3 and S2). The coatings appeared relatively smooth and uniform up to 10 wt % loading, with the nanoparticles becoming more evenly dispersed. The most uniform coating was observed at 10 wt % loading. At 20 wt % loading, particle aggregation became more pronounced, with large aggregates protruding out of the PDMS binder, making the film rougher. The uneven distribution of the nanoparticles at greater than 10 wt % loading may explain the slight decrease in biofilm inhibition observed in Figure 2. At 30 wt % loading and higher, the PDMS binder failed to adequately fill the voids in between the TiO_2 nanoparticles or their aggregates, as evidenced by the appearance of large holes on the surface, which was similarly observed by Xu *et al.*[52] This suggests that there is an optimal nanoparticle loading to achieve a uniform and smooth surface morphology for the PDMS/TiO_2 nanocomposite coatings.

The roughness parameters S_a and S_z have been suggested as useful surface parameters for comparing biomaterial surfaces in terms of microbial adhesion.[53] The S_a and S_z values (Figure 4) for the bare PDMS coating were 0.072 and 0.996 μm, respectively, similar to those obtained by De-la-Pinta et al.[54] Addition of up to 5 wt % TiO_2 increased S_a and S_z slightly; however, the increase was not statistically significant. Above 10 wt % TiO_2, these roughness parameters significantly increased (Figure 4). The average S_a values were 0.072, 0.094, 0.083, 0.137, and 0.275 μm for the 0, 2.5, 5, 9, and 13 wt % PDMS/TiO_2 nanocomposite coatings, respectively. The average S_z values were 0.996, 1.175, 1.018, 1.374, and 2.207 μm for the 0, 2.5, 5, 9, and 13 wt % PDMS/TiO_2 nanocomposite coatings, respectively. Research has shown a strong correlation between fungal and microbial adhesion and increased surface roughness. Rough surfaces provide more contact area, which is favorable for the process of biofilm formation.[54−58] However, even though the roughness increased between 2.5 and 13 wt % TiO_2 loadings, no further increase in fungal biofilm inhibition was observed, suggesting that roughness was likely not a major contributor to antibiofilm activity of the nanocomposite coating.

Wettability. The surface wettability of the nanocomposite PDMS/TiO_2 was evaluated via contact angle measurements of the nanocomposites before (called pristine) and after reactive oxygen plasma treatment (Figures 5 and S3) to measure surface hydrophobicity. All samples were allowed to rest for 48 hours before the water contact angle (WCA) measurements. The average WCA of pristine PDMS was about 110°, which agrees well with literature values of ∼100−120°.[45,59−61] Little change in the WCA was observed with the pristine samples because TiO_2 NPs are mostly covered with PDMS before the plasma treatment. The plasma-treated PDMS/TiO_2 samples exhibited hydrophobic recovery, a process in which hydrophilic silanol (Si−OH) groups created on the surface during the plasma treatment are passivated by un-cross-linked PDMS molecules that migrate from the bulk to the surface, rendering the PDMS surface hydrophobic again.[62−65] Inclusion of hydrophilic entities such as TiO_2 nanoparticles[66,67] seemed to impede the hydrophobic recovery process after plasma treatment,[68,69] even after more than 48 hours. For the plasma-treated samples, average contact angles were 96°, 57°, 45°, 46°, and 70° for the 0, 2.5, 5, 9, and 13 wt % PDMS/TiO_2 nanocomposite coatings, respectively. The WCA trend reversal for the 13 wt % coating could be due to increased aggregation and poor dispersion of TiO_2 nanoparticles, as seen in Figure 3, leading to the formation of TiO_2 aggregates and leaving behind large domains of bare PDMS that can undergo hydrophobic recovery. Overall, the inclusion of TiO_2 nanoparticles appeared to impede the hydrophobic recovery of PDMS.

https://doi.org/10.1021/acsomega.4c07869
ACS Omega 2024, 9, 42593−42601

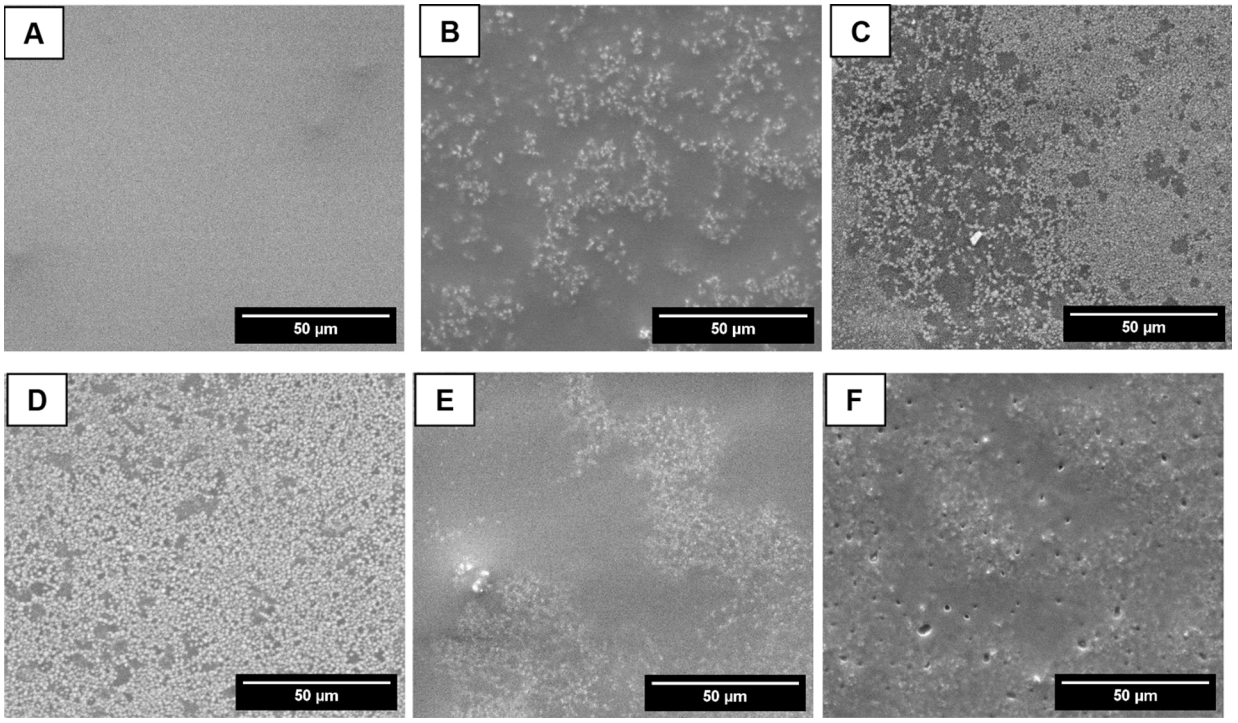

Figure 3. SEM images of the PDMS/TiO_2 coatings with (A) 0 wt % NPs, (B) 2.5 wt % NPs, (C) 5 wt % NPs, (D) 10 wt % NPs, (E) 20 wt % NPs, and (F) 30 wt % NPs.

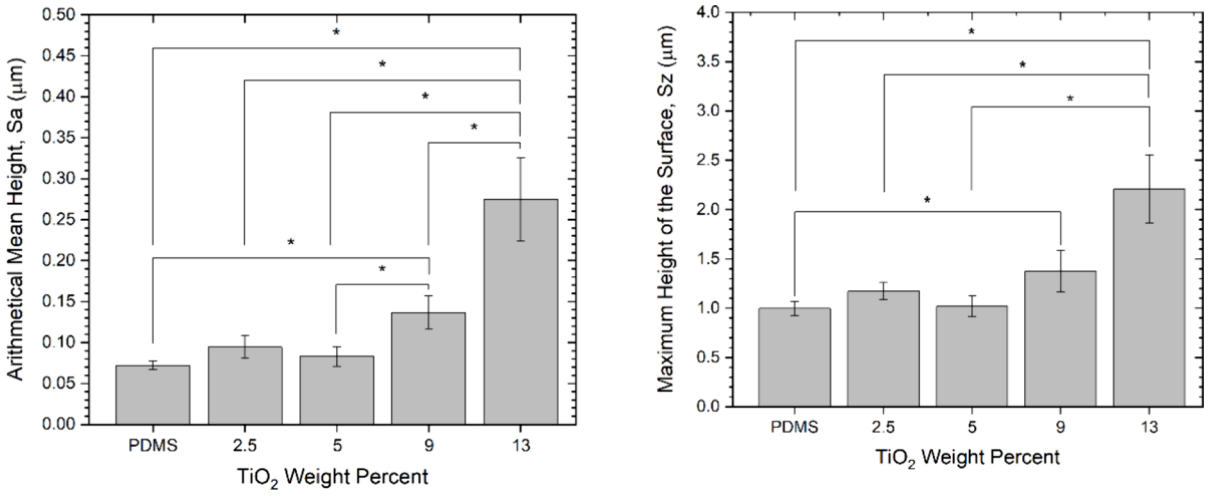

Figure 4. Surface roughness measurements of the PDMS/TiO_2 nanocomposite coatings as a function of NP weight loading with standard errors from at least 6 independent samples. *: statistically significantly different ($p < 0.05$, Student's t test).

Effects of Plasma Treatment on Biofilm Formation on the Nanocomposite. Cells were grown in RPMI 1640 media on the coated plates for 24 hours at 37 °C under LED incubation to assess the effects of plasma treatment of the nanocomposite on biofilm formation. Results showed a similar amount of biofilm formation across all samples without plasma treatment, with the nanoparticles having no effect on biofilm formation (see Figure 6). On the other hand, the plasma-treated samples exhibited significantly less biofilm formation in all conditions. Comparing plasma-treated to untreated plates, 2.5% TiO_2 nanoparticle samples had about a 75% reduction in the biofilm and the 5, 9, and 13 wt % TiO_2 nanoparticle samples had about 67% reduction on average after plasma treatment. Interestingly, plasma treatment of PDMS without TiO_2 nanoparticles also reduced biofilm formation by about 40%. The inhibition observed with the plasma-treated versus non-plasma-treated PDMS-only samples may be due to the temporarily increased hydrophilicity that hinders the adhesion of *C. glabrata* and other *Candida* species. Plasma-treated polymers, like PDMS, typically become more hydrophilic after exposure to high-energy plasma gas species, such as oxygen and nitrogen.[62] Due to the instability of the high-energy surface groups formed, the increased surface hydrophilicity is temporary and spontaneously reverts through the hydrophobic recovery process. The addition of TiO_2 nanoparticles to PDMS likely impedes hydrophobic recovery, increasing the longevity of its enhanced hydrophilicity.[69] This was supported by the observed correlation between wettability and biofilm for-

https://doi.org/10.1021/acsomega.4c07869
ACS Omega 2024, 9, 42593−42601

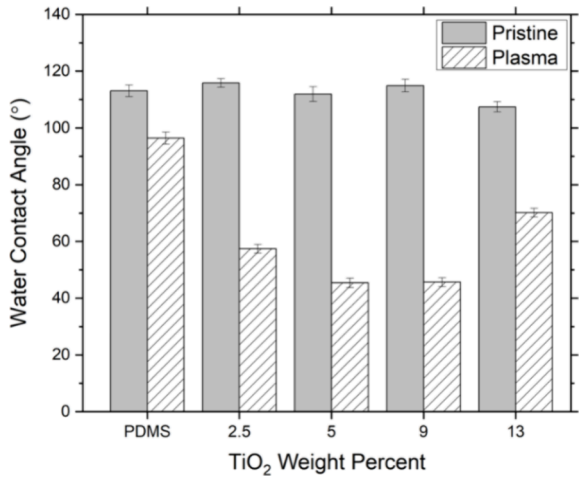

Figure 5. WCAs of the pristine and the oxygen plasma-treated PDMS/TiO_2 nanocomposite coatings as a function of NP weight loadings. Error bars are standard errors from three replicate sets of samples.

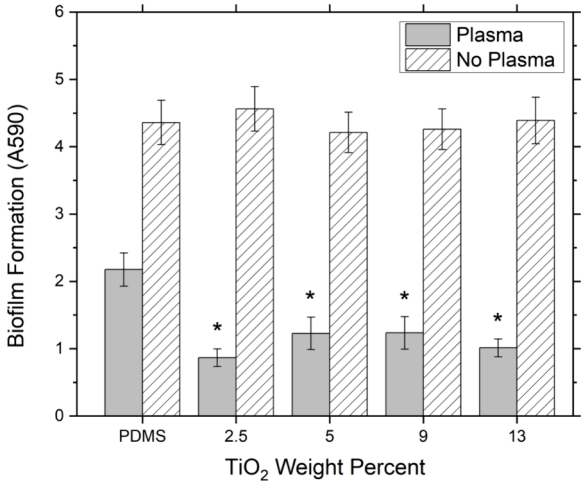

Figure 6. Impact of plasma treatment on TiO_2 coating against *C. glabrata* biofilm growth. The error bars represent the standard error from six biological replicates. *: statistically significantly different from its PDMS-only control (p-value < 0.05, Student's t test).

mation, where higher antibiofilm activities were observed for nanocomposite coatings with 2.5−9 wt % TiO_2 loading (Figures 5 and 6). The result is consistent with prior studies that showed adherence of *C. glabrata* to more hydrophobic surfaces,[70,71] which is mediated by the adhesin protein Epa6.[8,72] The reduced hydrophobic recovery in the nanocomposites likely prevents biofilm adhesion by forming a hydration layer, which acts as an energetic barrier against nonspecific fungal and bacterial protein adsorption onto the surface.[55,73−75]

CONCLUSIONS

Biofilm formation by fungal pathogens on surfaces poses infection risks. Previous works showed incorporating nanoparticles with known antimicrobial activities such as TiO_2 can inhibit biofilm formation in bacterial and fungal pathogens. Various possible mechanisms responsible for the antimicrobial activities such as ROS formation and surface properties have been explored. In this work, we developed a TiO_2/PDMS nanocomposite using *tert*-butyl alcohol as a substitute for traditional toxic solvents like hexane and xylene.[76−78] We show that the TiO_2/PDMS nanocomposites have strong antibiofilm properties against *C. glabrata*, and the antibiofilm activity is primarily due to reduced hydrophobicity of PDMS by the presence of TiO_2 nanoparticles and oxygen plasma treatment. *C. glabrata* has high resistance to oxidative stress, making ROS formation less effective as an antibiofilm strategy. Tuning surface properties, such as hydrophobicity, may be a more effective method for developing antibiofilm materials for biomedical applications.

ASSOCIATED CONTENT

Supporting Information

The Supporting Information is available free of charge at https://pubs.acs.org/doi/10.1021/acsomega.4c07869.

Representative spectra and images used in data analyses (PDF)

AUTHOR INFORMATION

Corresponding Authors

Katy C. Kao − *Department of Chemical and Materials Engineering, San Jose State University, San Jose 95112-3613 California, United States;* orcid.org/0000-0002-1184-276X; Email: dahyun.oh@sjsu.edu

Dahyun Oh − *Department of Chemical and Materials Engineering, San Jose State University, San Jose 95112-3613 California, United States;* orcid.org/0000-0003-1390-8440; Email: katy.kao@sjsu.edu

Authors

Khoi-Nguyen Nguyen − *Department of Chemical and Materials Engineering, San Jose State University, San Jose 95112-3613 California, United States;* orcid.org/0000-0003-4018-3545

Leena Sao − *Department of Chemical and Materials Engineering, San Jose State University, San Jose 95112-3613 California, United States*

Kevin Kyllo − *Department of Chemical and Materials Engineering, San Jose State University, San Jose 95112-3613 California, United States*

Danitza Hernandez − *Department of Chemical and Materials Engineering, San Jose State University, San Jose 95112-3613 California, United States*

Samantha Salomon − *Department of Chemical and Materials Engineering, San Jose State University, San Jose 95112-3613 California, United States*

Kalp Shah − *Department of Chemical and Materials Engineering, San Jose State University, San Jose 95112-3613 California, United States*

Complete contact information is available at: https://pubs.acs.org/10.1021/acsomega.4c07869

Notes

The authors declare no competing financial interest.

ACKNOWLEDGMENTS

This work was partially funded by NIH 1R16AI167832. The authors gratefully acknowledge the support of Christina Peters with SEM analysis, Neil Peters and Al Renaldo for the support with the reactive oxygen plasma treatment, and Heather Deshazer, Ayse Altunbas, Calvin Chen, and Calvin Kennell-

Heiling for the support with WCA and confocal laser scanning microscopy measurements.

REFERENCES

(1) Cavalheiro, M.; Teixeira, M. C. *Candida* Biofilms: Threats, Challenges, and Promising Strategies. *Front. Med.* **2018**, *5*, 28.
(2) d'Enfert, C.; Janbon, G. Biofilm Formation in *Candida glabrata*: What Have We Learnt from Functional Genomics Approaches? *FEMS Yeast Res.* **2016**, *16* (1), fov111.
(3) Rodrigues, C.; Rodrigues, M.; Silva, S.; Henriques, M. *Candida glabrata* Biofilms: How Far Have We Come? *J. Fungi* **2017**, *3* (1), 11.
(4) Salazar, S. B.; Simões, R. S.; Pedro, N. A.; Pinheiro, M. J.; Carvalho, M. F. N. N.; Mira, N. P. An Overview on Conventional and Non-Conventional Therapeutic Approaches for the Treatment of Candidiasis and Underlying Resistance Mechanisms in Clinical Strains. *J. Fungi* **2020**, *6* (1), 23.
(5) Adam, B.; Baillie, G. S.; Douglas, L. J. Mixed Species Biofilms of *Candida albicans* and *Staphylococcus epidermidis*. *J. Med. Microbiol.* **2002**, *51* (4), 344−349.
(6) Giles, C.; Lamont-Friedrich, S. J.; Michl, T. D.; Griesser, H. J.; Coad, B. R. The Importance of Fungal Pathogens and Antifungal Coatings in Medical Device Infections. *Biotechnol. Adv.* **2018**, *36* (1), 264−280.
(7) Harriott, M. M.; Noverr, M. C. *Candida albicans* and *Staphylococcus aureus* Form Polymicrobial Biofilms: Effects on Antimicrobial Resistance. *Antimicrob. Agents Chemother.* **2009**, *53* (9), 3914−3922.
(8) Olson, M. L.; Jayaraman, A.; Kao, K. C. Relative Abundances of *Candida albicans* and *Candida glabrata* in *In Vitro* Coculture Biofilms Impact Biofilm Structure and Formation. *Appl. Environ. Microbiol.* **2018**, *84* (8), No. e02769-17.
(9) Qayyum, S.; Khan, A. U. Nanoparticles *vs.* Biofilms: A Battle against Another Paradigm of Antibiotic Resistance. *MedChemComm* **2016**, *7* (8), 1479−1498.
(10) Zheng, S.; Bawazir, M.; Dhall, A.; Kim, H.-E.; He, L.; Heo, J.; Hwang, G. Implication of Surface Properties, Bacterial Motility, and Hydrodynamic Conditions on Bacterial Surface Sensing and Their Initial Adhesion. *Front. Bioeng. Biotechnol.* **2021**, *9*, No. 643722.
(11) Le, P. H.; Nguyen, D. H. K.; Aburto-Medina, A.; Linklater, D. P.; Crawford, R. J.; MacLaughlin, S.; Ivanova, E. P. Nanoscale Surface Roughness Influences *Candida albicans* Biofilm Formation. *ACS Appl. Bio Mater.* **2020**, *3* (12), 8581−8591.
(12) Izumida, F. E.; Moffa, E. B.; Vergani, C. E.; Machado, A. L.; Jorge, J. H.; Giampaolo, E. T. *In Vitro* Evaluation of Adherence of *Candida albicans*, *Candida glabrata*, and *Streptococcus mutans* to an Acrylic Resin Modified by Experimental Coatings. *Biofouling* **2014**, *30* (5), 525−533.
(13) Ahmadpour Kermani, S.; Salari, S.; Ghasemi Nejad Almani, P. Comparison of Antifungal and Cytotoxicity Activities of Titanium Dioxide and Zinc Oxide Nanoparticles with Amphotericin B against Different *Candida* Species: *In Vitro* Evaluation. *J. Clin. Lab. Anal.* **2021**, *35* (1), No. e23577.
(14) Alabdallah, N. M.; Irshad, M. A.; Rizwan, M.; Nawaz, R.; Inam, A.; Mohsin, M.; Khurshid, I.; Alharby, H. F.; Bamagoos, A. A.; Ali, S. Synthesis, Characterization and Antifungal Potential of Titanium Dioxide Nanoparticles against Fungal Disease (*Ustilago tritici*) of Wheat (*Triticum aestivum* L.). *Environ. Res.* **2023**, *228*, No. 115852.
(15) Altaf, M.; Zeyad, M. T.; Hashmi, M. A.; Manoharadas, S.; Hussain, S. A.; Ali Abuhasil, M. S.; Almuzaini, M. A. M. Effective Inhibition and Eradication of Pathogenic Biofilms by Titanium Dioxide Nanoparticles Synthesized Using *Carum copticum* Extract. *RSC Adv.* **2021**, *11* (31), 19248−19257.
(16) Anupong, W.; On-uma, R.; Jutamas, K.; Salmen, S. H.; Alharbi, S. A.; Joshi, D.; Jhanani, G. K. Antibacterial, Antifungal, Antidiabetic, and Antioxidant Activities Potential of *Coleus aromaticus* Synthesized Titanium Dioxide Nanoparticles. *Environ. Res.* **2023**, *216*, No. 114714.
(17) Tzeng, J.-H.; Weng, C.-H.; Chang, C.-J.; Yen, L.-T.; De Luna, M. D. G.; Huang, J.-W.; Lin, Y.-T. N-Schorl TiO_2 Nanocomposite for Visible-Light Photocatalysis Deactivation Yeast Exemplified by *Candida albicans*. *Chem. Eng. J.* **2022**, *435*, No. 134294.
(18) Foster, H. A.; Ditta, I. B.; Varghese, S.; Steele, A. Photocatalytic Disinfection Using Titanium Dioxide: Spectrum and Mechanism of Antimicrobial Activity. *Appl. Microbiol. Biotechnol.* **2011**, *90* (6), 1847−1868.
(19) Kubacka, A.; Diez, M. S.; Rojo, D.; Bargiela, R.; Ciordia, S.; Zapico, I.; Albar, J. P.; Barbas, C.; Martins Dos Santos, V. A. P.; Fernández-García, M.; Ferrer, M. Understanding the Antimicrobial Mechanism of TiO_2-Based Nanocomposite Films in a Pathogenic Bacterium. *Sci. Rep.* **2014**, *4* (1), 4134.
(20) Metryka, O.; Wasilkowski, D.; Mrozik, A. Evaluation of the Effects of Ag, Cu, ZnO and TiO_2 Nanoparticles on the Expression Level of Oxidative Stress-Related Genes and the Activity of Antioxidant Enzymes in *Escherichia coli*, *Bacillus cereus* and *Staphylococcus epidermidis*. *Int. J. Mol. Sci.* **2022**, *23* (9), 4966.
(21) Wasa, A.; Land, J. G.; Gorthy, R.; Krumdieck, S.; Bishop, C.; Godsoe, W.; Heinemann, J. A. Antimicrobial and Biofilm-Disrupting Nanostructured TiO_2 Coating Demonstrating Photoactivity and Dark Activity. *FEMS Microbiol. Lett.* **2021**, *368* (7), fnab039.
(22) Alberti, S.; Ferretti, M.; Vicini, S.; Castellano, M.; Caratto, V. Porous Polydimethylsiloxane Membranes Loaded with Low-Temperature Crystallized TiO_2 NPs for Detachable Antibacterial Films. *J. Mater. Sci.* **2019**, *54* (2), 1665−1676.
(23) Chobba, M. B.; Weththimuni, M. L.; Messaoud, M.; Urzi, C.; Bouaziz, J.; De Leo, F.; Licchelli, M. Ag-TiO_2/PDMS Nanocomposite Protective Coatings: Synthesis, Characterization, and Use as a Self-Cleaning and Antimicrobial Agent. *Prog. Org. Coat.* **2021**, *158*, No. 106342.
(24) Correa, C. F.; Santana, L. R.; Silva, R. M.; Noremberg, B. S.; Lund, R. G.; Ribeiro, J. S.; Motta, F. V.; Bomio, M. R. D.; Nascimento, R. M.; Carreño, N. L. V. Antimicrobial Activity from Polymeric Composites-Based Polydimethylsiloxane/TiO_2/GO: Evaluation of Filler Synthesis and Surface Morphology. *Polym. Bull.* **2017**, *74* (6), 2379−2390.
(25) Pawlus, P.; Reizer, R.; Wieczorowski, M. Functional Importance of Surface Texture Parameters. *Materials* **2021**, *14* (18), 5326.
(26) Huang, M.; Khan, J.; Kaur, M.; Vanega, J. D. T.; Patiño, O. A. A.; Ramasubramanian, A. K.; Kao, K. C. CgSTE11 Mediates Cross Tolerance to Multiple Environmental Stressors in *Candida glabrata*. *Sci. Rep.* **2019**, *9* (1), 17036.
(27) Houas, A. Photocatalytic Degradation Pathway of Methylene Blue in Water. *Appl. Catal. B Environ.* **2001**, *31* (2), 145−157.
(28) Xu, C.; Rangaiah, G. P.; Zhao, X. S. Photocatalytic Degradation of Methylene Blue by Titanium Dioxide: Experimental and Modeling Study. *Ind. Eng. Chem. Res.* **2014**, *53* (38), 14641−14649.
(29) Reddy, K. M.; Manorama, S. V.; Reddy, A. R. Bandgap Studies on Anatase Titanium Dioxide Nanoparticles. *Mater. Chem. Phys.* **2002**, *78* (1), 239−245.
(30) Wang, Y.; Sun, H.; Tan, S.; Feng, H.; Cheng, Z.; Zhao, J.; Zhao, A.; Wang, B.; Luo, Y.; Yang, J.; Hou, J. G. Role of Point Defects on the Reactivity of Reconstructed Anatase Titanium Dioxide (001) Surface. *Nat. Commun.* **2013**, *4* (1), 2214.
(31) Chen, S.; Xiao, Y.; Wang, Y.; Hu, Z.; Zhao, H.; Xie, W. A Facile Approach to Prepare Black TiO_2 with Oxygen Vacancy for Enhancing Photocatalytic Activity. *Nanomaterials* **2018**, *8* (4), 245.
(32) Zou, Y.; Yang, K.; Chen, Q.; Wang, H.; Meng, X. Molten Salt Construction of Stable Oxygen Vacancies on TiO_2 for Enhancement of Visible Light Photocatalytic Activity. *RSC Adv.* **2018**, *8* (64), 36819−36825.
(33) Dette, C.; Pérez-Osorio, M. A.; Kley, C. S.; Punke, P.; Patrick, C. E.; Jacobson, P.; Giustino, F.; Jung, S. J.; Kern, K. TiO_2 Anatase with a Bandgap in the Visible Region. *Nano Lett.* **2014**, *14* (11), 6533−6538.
(34) Liu, L.; Zhao, H.; Andino, J. M.; Li, Y. Photocatalytic CO_2 Reduction with H_2O on TiO_2 Nanocrystals: Comparison of Anatase, Rutile, and Brookite Polymorphs and Exploration of Surface Chemistry. *ACS Catal.* **2012**, *2* (8), 1817−1828.

https://doi.org/10.1021/acsomega.4c07869
ACS Omega 2024, 9, 42593−42601

(35) Bi, X.; Du, G.; Kalam, A.; Sun, D.; Yu, Y.; Su, Q.; Xu, B.; Al-Sehemi, A. G. Tuning Oxygen Vacancy Content in TiO_2 Nanoparticles to Enhance the Photocatalytic Performance. *Chem. Eng. Sci.* **2021**, *234*, No. 116440.
(36) Nakamura, I.; Negishi, N.; Kutsuna, S.; Ihara, T.; Sugihara, S.; Takeuchi, K. Role of Oxygen Vacancy in the Plasma-Treated TiO_2 Photocatalyst with Visible Light Activity for NO Removal. *J. Mol. Catal. Chem.* **2000**, *161* (1−2), 205−212.
(37) Park, S. Y.; Lee, H. U.; Ahn, K.; Kim, J. P.; Jin, J. S.; Lee, J.; Jeong, S. Y.; Cho, C. R. Enhanced Photocatalytic Activity of TiO_2-Incorporated Nanofiber Membrane by Oxygen Plasma Treatment. *Thin Solid Films* **2011**, *519* (20), 6899−6902.
(38) Epling, W. S.; Peden, C. H. F.; Henderson, M. A.; Diebold, U. Evidence for Oxygen Adatoms on TiO_2 (110) Resulting from O_2 Dissociation at Vacancy Sites. *Surf. Sci.* **1998**, *412*−*413*, 333−343.
(39) Setvín, M.; Aschauer, U.; Scheiber, P.; Li, Y.-F.; Hou, W.; Schmid, M.; Selloni, A.; Diebold, U. Reaction of O_2 with Subsurface Oxygen Vacancies on TiO_2 Anatase (101). *Science* **2013**, *341* (6149), 988−991.
(40) Zhang, Z.; Bondarchuk, O.; Kay, B. D.; White, J. M.; Dohnálek, Z. Imaging Water Dissociation on TiO_2 (110): Evidence for Inequivalent Geminate OH Groups. *J. Phys. Chem. B* **2006**, *110* (43), 21840−21845.
(41) Rangarajan, G.; Jayaseelan, A.; Farnood, R. Photocatalytic Reactive Oxygen Species Generation and Their Mechanisms of Action in Pollutant Removal with Biochar Supported Photocatalysts: A Review. *J. Clean. Prod.* **2022**, *346*, No. 131155.
(42) Setvin, M.; Franchini, C.; Hao, X.; Schmid, M.; Janotti, A.; Kaltak, M.; Van De Walle, C. G.; Kresse, G.; Diebold, U. Direct View at Excess Electrons in TiO_2 Rutile and Anatase. *Phys. Rev. Lett.* **2014**, *113* (8), No. 086402.
(43) Rahman, K. H.; Kar, A. K. Role of Bridging Oxygen Vacancy on Reduced Anatase TiO_2 (101) for Photodegradation of Rhodamine-B. *ECS J. Solid State Sci. Technol.* **2021**, *10* (11), 116004.
(44) Wang, C.; Böttcher, C.; Bahnemann, D. W.; Dohrmann, J. K. A Comparative Study of Nanometer Sized Fe(III)-Doped TiO_2 Photocatalysts: Synthesis, Characterization and Activity. *J. Mater. Chem.* **2003**, *13* (9), 2322−2329.
(45) Jiang, B.; Guo, H.; Chen, D.; Zhou, M. Microscale Investigation on the Wettability and Bonding Mechanism of Oxygen Plasma-Treated PDMS Microfluidic Chip. *Appl. Surf. Sci.* **2022**, *574*, No. 151704.
(46) Ruben, B.; Elisa, M.; Leandro, L.; Victor, M.; Gloria, G.; Marina, S.; Mian, K. S.; Pandiyan, R.; Nadhira, L. Oxygen Plasma Treatments of Polydimethylsiloxane Surfaces: Effect of the Atomic Oxygen on Capillary Flow in the Microchannels. *Micro Nano Lett.* **2017**, *12* (10), 754−757.
(47) Narayanasamy, J.; Kubicki, J. D. Mechanism of Hydroxyl Radical Generation from a Silica Surface: Molecular Orbital Calculations. *J. Phys. Chem. B* **2006**, *110* (32), 16158−16158.
(48) Cuéllar-Cruz, M.; Briones-Martin-del-Campo, M.; Cañas-Villamar, I.; Montalvo-Arredondo, J.; Riego-Ruiz, L.; Castaño, I.; De Las Peñas, A. High Resistance to Oxidative Stress in the Fungal Pathogen *Candida glabrata* Is Mediated by a Single Catalase, Cta1p, and Is Controlled by the Transcription Factors Yap1p, Skn7p, Msn2p, and Msn4p. *Eukaryot. Cell* **2008**, *7* (5), 814−825.
(49) Duggan, S.; Usher, J. *Candida glabrata*: A Powerhouse of Resistance. *PLOS Pathog.* **2023**, *19* (10), No. e1011651.
(50) Rodrigues, C. F.; Silva, S.; Henriques, M. *Candida glabrata*: A Review of Its Features and Resistance. *Eur. J. Clin. Microbiol. Infect. Dis.* **2014**, *33* (5), 673−688.
(51) Shantal, C.-J. N.; Juan, C.-C.; Lizbeth, B.-U. S.; Carlos, H.-G. J.; Estela, G.-P. B. *Candida glabrata* Is a Successful Pathogen: An Artist Manipulating the Immune Response. *Microbiol. Res.* **2022**, *260*, No. 127038.
(52) Xu, F.; Wang, T.; Bohling, J.; Maurice, A. M.; Chen, H.; Wu, L.; Zhou, S. Extended Hydrophobicity and Self-Cleaning Performance of Waterborne PDMS/TiO_2 Nanocomposite Coatings under Accelerated Laboratory and Outdoor Exposure Testing. *J. Coat. Technol. Res.* **2018**, *15* (5), 1025−1034.
(53) Etxeberria, M.; Escuin, T.; Vinas, M.; Ascaso, C. Useful Surface Parameters for Biomaterial Discrimination. *Scanning* **2015**, *37* (6), 429−437.
(54) De-la-Pinta, I.; Cobos, M.; Ibarretxe, J.; Montoya, E.; Eraso, E.; Guraya, T.; Quindós, G. Effect of Biomaterials Hydrophobicity and Roughness on Biofilm Development. *J. Mater. Sci. Mater. Med.* **2019**, *30* (7), 77.
(55) Fernández-Gómez, P.; Muro-Fraguas, I.; Múgica-Vidal, R.; Sainz-García, A.; Sainz-García, E.; González-Raurich, M.; Álvarez-Ordóñez, A.; Prieto, M.; López, M.; López, M.; Toledano, P.; Sáenz, Y.; González-Marcos, A.; Alba-Elías, F. Development and Characterization of Anti-Biofilm Coatings Applied by Non-Equilibrium Atmospheric Plasma on Stainless Steel. *Food Res. Int.* **2022**, *152*, No. 109891.
(56) Schubert, A.; Wassmann, T.; Holtappels, M.; Kurbad, O.; Krohn, S.; Bürgers, R. Predictability of Microbial Adhesion to Dental Materials by Roughness Parameters. *Coatings* **2019**, *9* (7), 456.
(57) Teughels, W.; Van Assche, N.; Sliepen, I.; Quirynen, M. Effect of Material Characteristics and/or Surface Topography on Biofilm Development. *Clin. Oral Implants Res.* **2006**, *17* (S2), 68−81.
(58) Verran, J.; Lees, G.; Shakespeare, A. P. The Effect of Surface Roughness on the Adhesion of *Candida albicans* to Acrylic. *Biofouling* **1991**, *3* (3), 183−191.
(59) Bodas, D.; Rauch, J.-Y.; Khan-Malek, C. Surface Modification and Aging Studies of Addition-Curing Silicone Rubbers by Oxygen Plasma. *Eur. Polym. J.* **2008**, *44* (7), 2130−2139.
(60) Eddington, D. T.; Puccinelli, J. P.; Beebe, D. J. Thermal Aging and Reduced Hydrophobic Recovery of Polydimethylsiloxane. *Sens. Actuators B Chem.* **2006**, *114* (1), 170−172.
(61) O'Brien, D. J.; Sedlack, A. J. H.; Bhatia, P.; Jensen, C. J.; Quintana-Puebla, A.; Paranjape, M. Systematic Characterization of Hydrophilized Polydimethylsiloxane. *J. Microelectromechanical Syst.* **2020**, *29* (5), 1216−1224.
(62) Bhandaru, N.; Agrawal, N.; Banik, M.; Mukherjee, R.; Sharma, A. Hydrophobic Recovery of Cross-Linked Polydimethylsiloxane Films and Its Consequence in Soft Nano Patterning. *Bull. Mater. Sci.* **2020**, *43* (1), 186.
(63) Fritz, J. L.; Owen, M. J. Hydrophobic Recovery of Plasma-Treated Polydimethylsiloxane. *J. Adhes.* **1995**, *54* (1−4), 33−45.
(64) Hillborg, H.; Sandelin, M.; Gedde, U. W. Hydrophobic Recovery of Polydimethylsiloxane after Exposure to Partial Discharges as a Function of Crosslink Density. *Polymer* **2001**, *42* (17), 7349−7362.
(65) Owen, M. J.; Smith, P. J. Plasma Treatment of Polydimethylsiloxane. *J. Adhes. Sci. Technol.* **1994**, *8* (10), 1063−1075.
(66) Bolis, V.; Busco, C.; Ciarletta, M.; Distasi, C.; Erriquez, J.; Fenoglio, I.; Livraghi, S.; Morel, S. Hydrophilic/Hydrophobic Features of TiO_2 Nanoparticles as a Function of Crystal Phase, Surface Area and Coating, in Relation to Their Potential Toxicity in Peripheral Nervous System. *J. Colloid Interface Sci.* **2012**, *369* (1), 28−39.
(67) Hao, Y.-Q.; Wang, Y.-F.; Weng, Y.-X. Particle-Size-Dependent Hydrophilicity of TiO_2 Nanoparticles Characterized by Marcus Reorganization Energy of Interfacial Charge Recombination. *J. Phys. Chem. C* **2008**, *112* (24), 8995−9000.
(68) Klonos, P.; Pissis, P.; Kyritsis, A. Effects of Hydration/Dehydration on Interfacial Polymer Fraction and Dynamics in Nanocomposites Based on Metal−Oxides and Physically Adsorbed Polymer. *J. Phys. Chem. C* **2017**, *121* (35), 19428−19441.
(69) Tsuzuki, T.; Baassiri, K.; Mahmoudi, Z.; Perumal, A. S.; Rajendran, K.; Rubies, G. M.; Nicolau, D. V. Hydrophobic Recovery of PDMS Surfaces in Contact with Hydrophilic Entities: Relevance to Biomedical Devices. *Materials* **2022**, *15* (6), 2313.
(70) Cavalheiro, M.; Pereira, D.; Formosa-Dague, C.; Leitão, C.; Pais, P.; Ndlovu, E.; Viana, R.; Pimenta, A. I.; Santos, R.; Takahashi-Nakaguchi, A.; Okamoto, M.; Ola, M.; Chibana, H.; Fialho, A. M.; Butler, G.; Dague, E.; Teixeira, M. C. From the First Touch to Biofilm

https://doi.org/10.1021/acsomega.4c07869
ACS Omega 2024, 9, 42593−42601

Establishment by the Human Pathogen Candida Glabrata: A Genome-Wide to Nanoscale View. *Commun. Biol.* **2021**, *4* (1), 886.
(71) Klotz, S. A.; Drutz, D. J.; Zajic, J. E. Factors Governing Adherence of *Candida* Species to Plastic Surfaces. *Infect. Immun.* **1985**, *50* (1), 97−101.
(72) El-Kirat-Chatel, S.; Beaussart, A.; Derclaye, S.; Alsteens, D.; Kucharíková, S.; Van Dijck, P.; Dufrêne, Y. F. Force Nanoscopy of Hydrophobic Interactions in the Fungal Pathogen *Candida glabrata*. *ACS Nano* **2015**, *9* (2), 1648−1655.
(73) Cheng, G.; Zhang, Z.; Chen, S.; Bryers, J. D.; Jiang, S. Inhibition of Bacterial Adhesion and Biofilm Formation on Zwitterionic Surfaces. *Biomaterials* **2007**, *28* (29), 4192−4199.
(74) Faustino, C. M. C.; Lemos, S. M. C.; Monge, N.; Ribeiro, I. A. C. A Scope at Antifouling Strategies to Prevent Catheter-Associated Infections. *Adv. Colloid Interface Sci.* **2020**, *284*, No. 102230.
(75) Zhang, H.; Chiao, M. Anti-Fouling Coatings of Poly-(Dimethylsiloxane) Devices for Biological and Biomedical Applications. *J. Med. Biol. Eng.* **2015**, *35* (2), 143−155.
(76) Alder, C. M.; Hayler, J. D.; Henderson, R. K.; Redman, A. M.; Shukla, L.; Shuster, L. E.; Sneddon, H. F. Updating and Expanding GSK's Solvent Sustainability Guide. *Green Chem.* **2016**, *18* (13), 3879−3890.
(77) Koschwanez, J. H.; Carlson, R. H.; Meldrum, D. R. Thin PDMS Films Using Long Spin Times or Tert-Butyl Alcohol as a Solvent. *PLoS One* **2009**, *4* (2), No. e4572.
(78) Lee, J. N.; Park, C.; Whitesides, G. M. Solvent Compatibility of Poly(Dimethylsiloxane)-Based Microfluidic Devices. *Anal. Chem.* **2003**, *75* (23), 6544−6554.

https://doi.org/10.1021/acsomega.4c07869
ACS Omega 2024, 9, 42593−42601